Open Access Full Text Article

ORIGINAL RESEARCH

Promoted Abutment-Soft Tissue Integration Around Self-Glazed Zirconia Surfaces with Nanotopography Fabricated by Additive 3D Gel Deposition

Chaoyi Huang[1,2], Xinchao Miao [1,2], Jiang Li[1,2], Jieyi Liang[1,2], Junxi Xu[1,2], Zhe Wu[1,2]

[1]Department of Prosthodontics, Affiliated Stomatology Hospital of Guangzhou Medical University, Guangzhou, People's Republic of China; [2]Guangdong Engineering Research Center of Oral Restoration and Reconstruction, Guangzhou Key Laboratory of Basic and Applied Research of Oral Regenerative Medicine, Guangzhou, People's Republic of China

Correspondence: Zhe Wu, Department of Prosthodontics, Affiliated Stomatology Hospital of Guangzhou Medical University, No. 39, Huangsha Road, Guangzhou, People's Republic of China, Tel +86 020 8850 1980, Fax +86 020 8850 1980, Email zhewudentist@gzhmu.edu.cn

Introduction: Improving the biological sealing around dental abutments could promote the long-term success of implants. Although titanium abutments have a wide range of clinical applications, they incur esthetic risks due to their color, especially in the esthetic zone. Currently, zirconia has been applied as an esthetic alternative material for implant abutments; however, zirconia is purported to be an inert biomaterial. How to improve the biological activities of zirconia has thus become a popular research topic. In this study, we presented a novel self-glazed zirconia (SZ) surface with nanotopography fabricated by additive 3D gel deposition and investigated its soft tissue integration capability compared to that of clinically used titanium and polished conventional zirconia surfaces.

Materials and Methods: Three groups of disc samples were prepared for in vitro study and the three groups of abutment samples were prepared for in vivo study. The surface topography, roughness, wettability and chemical composition of the samples were examined. Moreover, we analyzed the effect of the three groups of samples on protein adsorption and on the biological behavior of human gingival keratinocytes (HGKs) and human gingival fibroblasts (HGFs). Furthermore, we conducted an in vivo study in which the bilateral mandibular anterior teeth of rabbits were extracted and replaced with implants and corresponding abutments.

Results: The surface of SZ showed a unique nanotopography with nm range roughness and a greater ability to absorb protein. The promoted expression of adhesion molecules in both HGKs and HGFs was observed on the SZ surface compared to the surfaces of Ti and PCZ, while the cell viability and proliferation of HGKs and the number of HGFs adhesion were not significant among all groups. In vivo results showed that the SZ abutment formed strong biological sealing at the abutment–soft tissue interface and exhibited markedly more hemidesmosomes when observed with a transmission electron microscope.

Conclusion: These results demonstrated that the novel SZ surface with nanotopography promoted soft tissue integration, suggesting its promising application as a zirconia surface for the dental abutment.

Keywords: dental abutment, self-glazed zirconia, nanotopography, adhesion molecule, soft tissue integration, 3D gel deposition

Introduction

Well-organized soft tissue integration around dental implants is crucial to the long-term success of the implants and protects the implants from the invasion of oral microorganisms while also maintaining the esthetics of soft tissue.[1–4] Titanium is currently the first-choice material for dental implants,[5] but it may demonstrate a gray metal color or unwanted inflammatory responses with peri-implant soft tissue.[6,7] Recently, zirconia, as an alternative, has increased in popularity owing to its esthetic benefits over titanium.[8–10] However, the inert surface of zirconia affects its biological activity and thus the long-term success of zirconia dental implants, so various modification strategies such as physical, chemical, and biological have been explored to enhance the bioactivity of zirconia dental implants.[11–17] Currently, nanoengineering has been reported to simulate the surface properties of natural tissues to improve surface biological activity, especially with respect to surface topography.[18–22]

3141

With the constant evolution of ceramic materials to meet the higher criteria for aesthetics and biocompatibility and achieve long-term effects, a novel monolithic zirconia, referred to as self-glazed zirconia (SZ), fabricated by additive 3D gel deposition, has been developed and put on the market.[23,24] Remarkably, the surface of SZ with a unique nanotopography is formed by nanometer particles during the manufacturing process. Many studies have proven that nanotopography can not only improve the biological activities of surfaces but also play a certain role in the regulation of bacterial adhesion.[25–30] Moreover, this material exhibits an enamel-like outer surface that is smoother than that of conventional zirconia and can be used directly without any further manual processing. It showed a higher accuracy and fitness as well as reduced wear to tooth enamel,[26,31] and was widely used in the clinic for crown restoration, achieving a high level of evaluation by physicians and patients.[25,32] However, the study of SZ surface in the field of abutment is currently limited, and it remains unclear whether its nanotopographical surface can achieve soft tissue biological sealing.

Thus, the aim of this paper was to compare the soft tissue sealing effects of three groups of commercial dental materials, titanium, conventional zirconia and the novel self-glazed zirconia introduced above, to determine whether the nanotopography of SZ promotes soft tissue integration compared to commonly used abutments in clinical practice. Specifically, we hypothesized that the nanotopographical surface of SZ can regulate the adsorption of proteins and the behaviors of epithelial cells and fibroblasts and then enhance soft tissue integration around the implant.

Materials and Methods
Sample Preparation and Characterization
Disc samples with dimensions of 15 × 15 × 1 mm were prepared in vitro (Figure 1A), and abutment samples with a diameter of 4 mm and a height of 4.5 mm were prepared in vivo (Figure 2A). Three kinds of commercially available surfaces were investigated in the study as follows: titanium surface (Ti; Jiahong, Shenzhen, China), polished conventional zirconia surface (PCZ; Erran, Hanzhou, China) shaped by milling partially sintered blanks, and self-glazed zirconia surface (SZ; Erran, Hanzhou, China) manufactured by the precision additive 3D gel deposition approach.[31] In accordance with the requirements of clinical application, the manufacturers polished the titanium surface and conventional zirconia surface to 2500 mesh with gradient silicon carbide sandpapers while the SZ surface is not subject to polishing treatment. The preparation of each group of samples is completed by the same manufacturer. In addition, titanium implants with biphasic calcium phosphate surface treatment (Anthogyr, Sallanches, France) (3.4 mm diameter, 8 mm length) were utilized in vivo. All samples were cleaned ultrasonically in ethanol, deionized water, and ultrapure water sequentially and dried at room temperature. All groups were sterilized by autoclaving prior to further experimentation.

The surface topographies were characterized using scanning electron microscopy (SEM; Sigma 300, Zeiss, Germany) with an acceleration voltage of 3 kV. Atomic force microscopy (AFM; Dimension ICON, Bruker, Germany) was applied to observe the 3D topographies and measure the surface roughness within a 5 μm×5 μm area. The surface wettability was detected with a surface contact angle meter (WCA; YJ-82C, Ding Sheng, China) and tested with 5 μL of sessile distilled water droplets. The chemical composition of the three sample surfaces were determined by energy dispersive spectrometer (EDS; Model 550i, IXRF, USA). The experiments were conducted in triplicate, and the means ± standard deviations of two independent experiments were calculated.

Detection of Protein Adsorption Behavior
All samples were placed in 24-well plates with 1 mL of bovine serum albumin (BSA) dissolved in ultrapure water (2 mg/mL) (Figure 1B). Then, 1 mL BSA solution was added to each well and incubated at 37 °C with shaking (15 rpm/min). After 2 h, all samples were rinsed gently with ultrapure water twice to remove the nonadsorbed proteins. Then, 200 μL radioimmunoprecipitation assay (RIPA) buffer was added to each well to desorb the adsorbed protein from the sample surfaces at room temperature. Finally, the protein solution was collected and quantified with a Micro BCA™ protein assay kit (Thermo Fisher, Waltham, USA), and the absorbance values were measured by enzyme-labeled instrument (Multishan PC, Thermo Fisher, USA) at 562 nm.
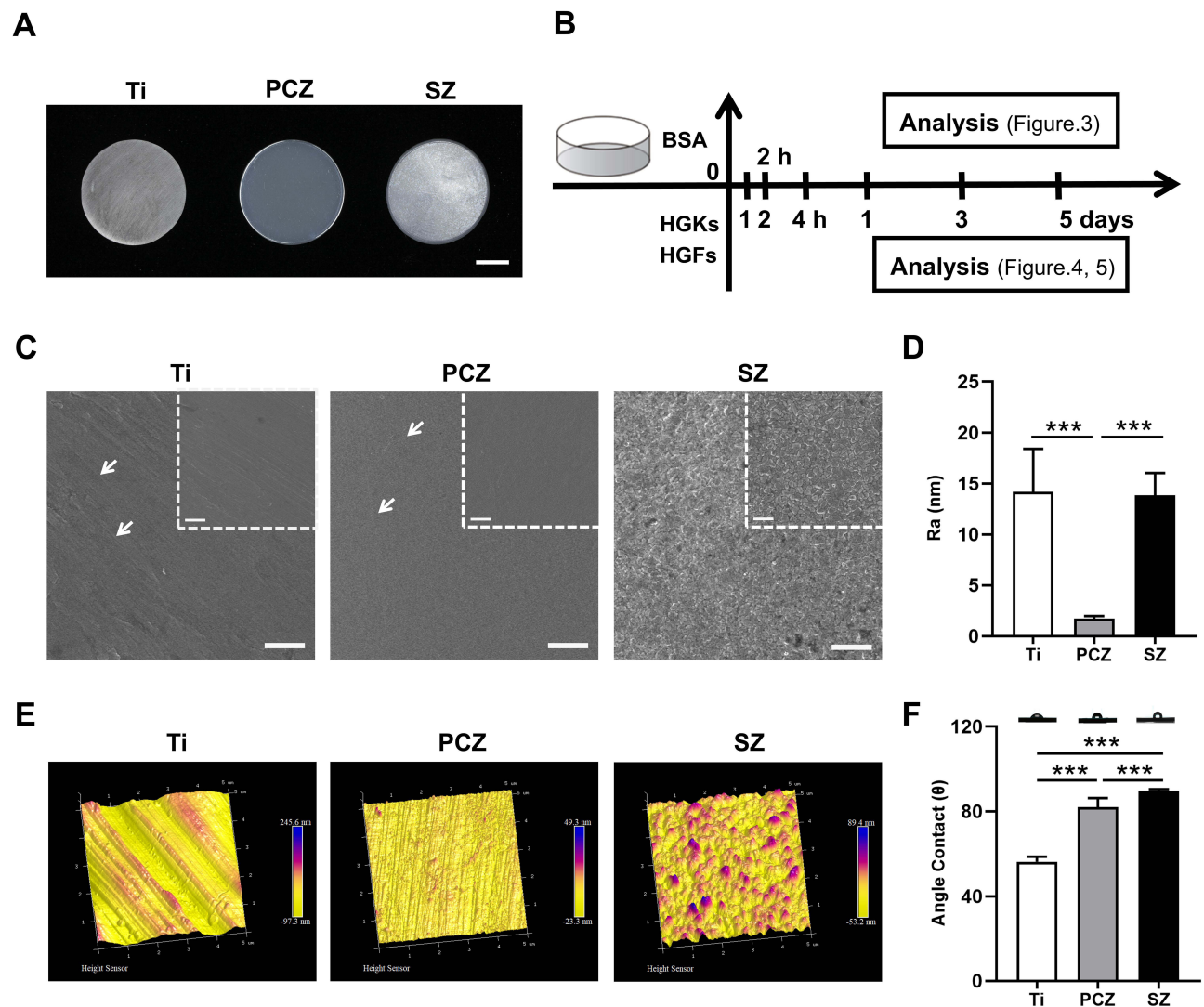
Figure 1 Surface characterizations and analysis of Ti, PCZ, and SZ samples. (**A** and **B**) Photographs of Ti, PCZ and SZ disc samples (scale bar = 5mm) and in vitro experimental design. (**C**) SEM images show the topography of sample surfaces, the arrows indicate the scratches on the surface (top: scale bar=1μm, bottom: scale bar=2μm). (**D**) Surface roughness measured by AFM, n=3. (**E**) AFM images show the 3D topography of sample surfaces. (**F**) Surface wettability analyzed by the water contact angle, n=3. ***$p<0.001$.

Similarly, fluorescein isothiocyanate (FITC)-BSA (Solarbio, Beijing, China) was dissolved in ultrapure water at the same concentration (2 mg/mL), and all group surfaces were soaked for 2 h and observed with upright fluorescence microscopy (BX43, Olympus, Japan) in the dark.

Biological Assessments in vitro

Human gingival keratinocytes (HGKs) and human gingival fibroblasts (HGFs) (iCell Bioscience, Shanghai, China) were seeded onto Ti, PCZ and SZ samples in 24-well plates (Figure 1B). Both HGKs and HGFs were cultured in standard culture medium (DMEM supplemented with 10% FBS and 1% antibiotics (streptomycin 100 U/mL, penicillin 100 U/mL)). The HGKs (4×10^4 cells/well) or HGFs (2×10^4 cells/well) were seeded onto sample surfaces and incubated for 1, 2, and 4 h to evaluate cell adhesion and morphology. Then, the HGKs (2×10^4 cells/well) and HGFs (1×10^4 cells/well) were seeded onto different surfaces with culture media replaced every 2 days, and the cell viability and cell proliferation were measured after 1, 3, and 5 days. After incubation for 3 days, immunofluorescence (IF) staining of collagen-I (Col-I) and fibronectin (FN) was performed on the HGFs. To evaluate adhesion molecule expression, the adhesion-related genes, including Laminin α3 (*Ln α3*), Laminin β3 (*Ln β3*), Laminin γ2 (*Ln γ2*) and Integrin α6 (*In α6*) of HGKs and *Col-I* and
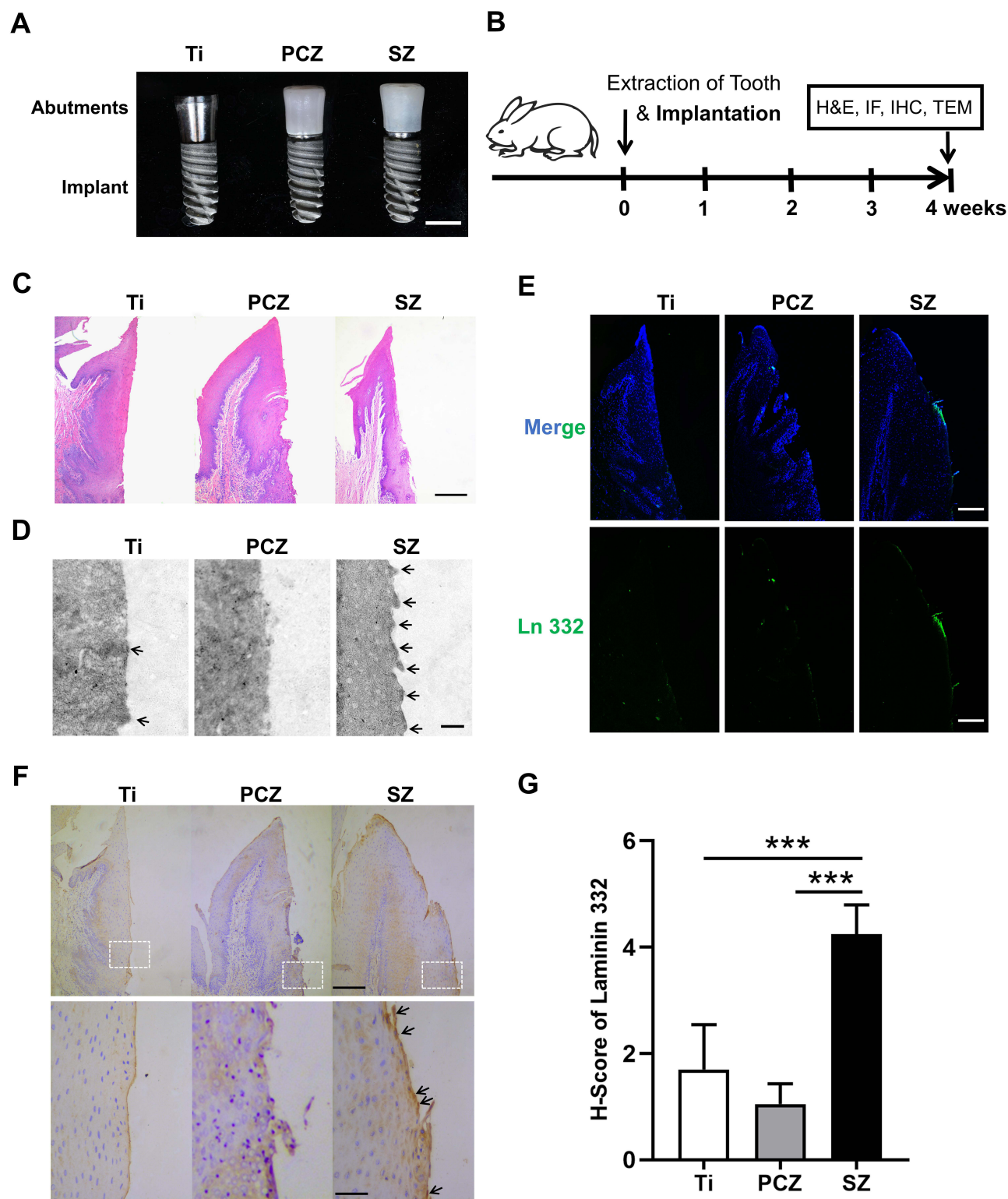
Figure 2 Soft tissue integration around Ti, PCZ, and SZ abutment samples (on the right is the abutment-soft tissue interface). (**A** and **B**) Photographs of the Ti, PCZ, and SZ abutments with implants (scale bar = 4 mm) and experimental protocol for in vivo study. (**C**) Morphology of soft tissue healing around the abutments by H&E stain (scale bar=200 μm). (**D**) Hemidesmosomes under TEM, the arrows indicate the hemidesmosome structures (scale bar=400 nm). (**E**) IF staining of Ln 332; Ln 332 (green), nuclei (blue), (scale bar=200μm), n=4. (**F, G**) IHC staining of Ln 332, the arrows indicate Ln 332 (top: scale bar=200μm, bottom: scale bar=50 μm), n=4. ***$p<0.001$.

FN of HGFs were detected by real-time quantitative polymerase chain reaction (RT–qPCR), and the expression of adhesion-related proteins, including Laminin 332 (Ln 332), In α6, Integrin β4 (In β4) of HGKs and Col-I and FN of HGFs was detected by Western blotting.

Protocol for the Cell Experiment

At the indicated time points after seeding, cells were fixed in 4% paraformaldehyde (PFA) and incubated with 4',6-diamidino-2-phenylindole (DAPI) for 10 min. Inverted fluorescence microscopy (DM13008/DF0450, Leica, Germany) was used to observe the DAPI-stained adherent nuclei. Ten fields of view were randomly selected per sample, and nuclei were counted using ImageJ (Maryland, USA) to evaluate cell adhesion. For cell morphology observation, cells were fixed and treated with 0.5% Triton X-100 at room temperature, incubated with phalloidin Alexa488 (Servicebio, Wuhan, China) for 1 h in the dark at 37°C and subsequently stained with DAPI for 10 min. Images were obtained using an upright fluorescence microscope.

The cell viability of the surfaces was measured via a Cell Counting Kit-8 (CCK-8; Dojindo, Kyushu, Japan). Each well was filled with 220 μL CCK-8 solution (200 μL medium and 20 μL of CCK-8). After incubation at 37°C for 2 h, 100 μL of CCK-8 solution was transferred to a 96-well plate, and the absorbance was detected using an enzyme-labeled instrument at 450 nm. Then, an EdU cell proliferation kit with Alexa Fluor 488 (Beyotime, Shanghai, China) was used to assess cell proliferation according to the manufacturer's protocol. Briefly, cells were incubated with EdU-labeled medium for 2 h, fixed with 4% PFA for 10 min, and permeabilized with 0.5% Triton X-100 for another 10 min. Then, all samples were stained with a click-reaction mixture at room temperature for 30 min and with Hoechst solution for 10 min in the dark. The results were visualized using an inverted fluorescence microscope. Six images were randomly obtained for each sample and analyzed with ImageJ.

Similarly, for IF staining, the samples were blocked with 5% BSA and incubated overnight with rabbit anti-Col-I (Abcam, Cambridge, USA) and rabbit anti-FN (Abcam, Cambridge, USA) at 4°C after the routine fixation and permeabilization of the cells. The next day, the cells were incubated with the corresponding fluorescently labeled secondary antibodies (Bioss, Beijing, China) for 1 h at 37°C. The cytoskeleton was stained with phalloidin Alexa 488, and the nuclei were counterstained with DAPI. Images were acquired via upright fluorescence microscopy.

For qRT–PCR, total RNA was extracted with the SteadyPure Universal RNA Extraction Kit (Accurate Biology, Hunan, China). A NanoDrop spectrophotometer (NanoDrop 2000, Wilmington, USA) was used to analyze the concentration and quality of RNA. Then, cDNA was obtained by reverse transcription using Evo M-MLV RT Premix (Accurate Biology, Hunan, China). Finally, real-time RT–PCR was performed using the SYBR® Green Premix Pro Taq HS qPCR Kit (Accurate Biology, Hunan, China) on the Bio-Rad Real-Time System (CFX96, Hercules, CA, USA). *GAPDH* was used as a housekeeping gene, and the sequences of the primers used in this study are shown in Table 1.

Cells were lysed in RIPA buffer, and total proteins were separated by SDS–PAGE and transferred onto polyvinylidene fluoride (PVDF) membranes for Western blot experiments. Then, the membrane was blocked for 1 h with 5% nonfat milk in the tris buffered saline with tween (TBST) at room temperature and incubated at 4°C overnight with one of the following primary antibodies: Ln 332 (Abcam, Cambridge, USA), In α6 (Santa Cruz, California, USA), In β4 (Abcam, Cambridge, USA), Col-I, FN

Table 1 Primers Used for Real-Time Polymerase Chain Reaction

Gene	Forward Primer Sequence (5'-3')	Reverse Primer Sequence (5'-3')
Ln α3	CACCGGGATATTTCGGGAATC	AGCTGTCGCAATCATCACATT
Ln β3	CCAAAGGTGCGACTGCAATG	AGTTCTTGCCTTCGGTGTGG
Ln γ2	CAAAGGTTCTCTTAGTGCTCGAT	CACTTGGAGTCTAGCAGTCTCT
In α6	CAGTGGAGCCGTGGTTTTG	CCACCGCCACATCATAGCC
Fn	CGGTGGCTGTCAGTCAAAG	AAACCTCGGCTTCCTCCATAA
Col-I	GAGGGCCAAGACGAAGACATC	CAGATCACGTCATCGCACAAC
GAPDH	GGACCTGACCTGCCGTCTAG	GTAGCCCAGGATGCCCTTGA

and GAPDH (Proteintech, Wuhan, China). Subsequently, the membranes were incubated with HRP-labeled secondary antibodies (Proteintech, Wuhan, China) for 1 h at room temperature and visualized using an ECL system (BLT, Guangzhou, China).

Biological Assessments in vivo
Animal Experiment and Tissue Preparation
Animals were maintained in accordance with animal care guidelines established by the Laboratory Animal Ethics Committee of Guangdong Huawei Testing Co., LTD (approval number: 202203004). Four-month-old male New Zealand white rabbits (n = 4, each group) (weighing 2.5–3 kg) were used in vivo (Figure 2B). In brief, bilateral mandibular anterior teeth were carefully extracted under general anesthesia with 0.1 mL/kg Sumianxin (Baite, Changsha, China) and 0.1 mL/kg Zoletil (Virbac, Carros, France). Then, the implants and corresponding experimental abutments were screwed into the extraction socket with a torque of 15 Ncm after washing with normal saline. Following surgery, animals were treated with gentamicin (0.05 mg/kg intramuscular injection) as an anti-inflammatory agent for 3 days. The experimental animals were kept and given food and water until euthanasia at 4 weeks following implantation. At the indicated time, the animals were sacrificed, and their mandibles, including implants, abutments, and peri-implant tissues, were removed and immersed in 4% PFA for 24 h and then in 5% ethylene diamine tetra-acetic acid (EDTA) for 4 days at 4°C. The peri-implant soft tissue was dissected gently with tweezers after stirring in a magnetic agitator at 4°C for 24 h.[33] The tissue specimens for histological staining were prepared by gradient dehydration and embedding. In addition, the tissue specimens for transmission electron microscopy (TEM; HT7800/ HT7700, Hitachi, Japan) observation were fixed at 4°C overnight in 2.5% glutaraldehyde solution.

Histological Evaluation
The paraffin-embedded specimens were cut into 4 μm sections. These sections were hydrated with gradient alcohol, stained with hematoxylin and eosin (H&E) and finally sealed with neutral gum. Histological changes were observed under a light microscope (M4300, Leica, Germany).

Hemidesmosomes Detection
Tissue specimens were fixed with 1% OsO4 in 0.1 M PBS (pH 7.4) for 2 h at room temperature in the dark. Then, they were treated with ethanol gradient dehydration, resin permeation, and embedding and finally prepared at room temperature. The resin blocks were cut to a thickness of 60–80 nm with an ultramicrotome, and the specimens were placed onto 150 mesh cuprum grids with formvar film. A 2% uranium acetate saturated alcohol solution was used to prevent light staining for 8 min, and 2.6% lead citrate was used to prevent CO_2 staining for 8 min. After drying with filter paper, the cuprum grids were placed into a grid board and dried overnight at room temperature. The cuprum grids were observed under transmission electron microscope (TEM), and images were taken.

Immunohistochemical and IF Staining
Tissue sections were incubated with sodium citrate antigenic repair fluid (Beyotime, Shanghai, China) in a pressure cooker for 10 min to retrieve the antigen and naturally cooled. After blocking endogenous peroxidase at 37°C for 30 min in 3% H_2O_2-methanol solution (Boster, Wuhan, China), 5% BSA was used to block tissue sections for 30 min at room temperature, and an antibody against Ln 332 (Bioss, Beijing, China) was incubated with slides overnight at 4°C. The next day, the sections were treated with goat anti-rabbit IgG for 45 minutes at room temperature and treated with 3,3'-diaminobenzidine (DAB) coloring kit (ZSGB-BIO, Beijing, China). After staining with hematoxylin, images were captured using a light microscope. It was scored separately using a 4-grade assessment of intensity (0 no staining, 1+ weak staining, 2+ moderate staining, 3+ strong staining).

In the same way, the sections were incubated with primary antibody to Ln 332 overnight at 4°C. The next day, these sections were incubated with fluorescently labeled secondary antibodies (Bioss, Beijing, China) at room temperature for 1 h. Finally, the sections were stained with DAPI and observed via inverted fluorescence microscopy.

Statistical Analysis
For all statistical analyses, GraphPad software version 8 (GraphPad Software; La Jolla, CA, USA) was used. The data are expressed as the means ± standard deviations (SDs). Differences between groups were analyzed using analysis of variance (ANOVA). A p-value of < 0.05 was considered statistically significant.

Results

Surface Characteristics and Analysis

The qualitative surface topography analysis (images) of the three groups of samples studied in this experiment is illustrated in Figure 1C. The surfaces of Ti and PCZ were relatively flat, although with some visible scratches. The surface of SZ had a dense and relatively uniform nano-protuberance, with small particle size, clear particle boundaries, and tight particle bonding. Therefore, the polishing treatment flattened the surfaces of both Ti and PCZ so that there was no obvious surface topography, while the surface of SZ had a unique nanotopography.

The AFM data shown in Figure 1E are in good agreement with the Ra values (Figure 1D). The surface roughness of PCZ was the lowest (Ra: 1.74 ±0.25 nm) ($P < 0.001$) and was significantly different from that of Ti (Ra: 14.19 ±4.22 nm) and SZ (Ra: 13.86 ±2.19 nm). However, the Ra values are all within nm ranges, reflecting significant but very small differences in roughness among the three groups of surfaces.

The wettability measurements are presented in Figure 1F. The water contact angles of the Ti, PCZ, and SZ surfaces were 56.25±2.43°, 82.09±4.24°, and 89.81±0.63°, respectively. The Ti surface was obviously more hydrophilic, while the surfaces of PCZ and SZ were relatively hydrophobic, and there were significant differences among the groups ($P < 0.001$). The chemical composition data of the three groups samples are shown in Table 2 and Supplementary Figure 1. The Ti surface was mainly composed of nitrogen, oxygen and titanium, while the surface of PCZ and SZ were mainly composed of carbon, oxygen and zirconium with a similar ratio.

Adsorption Behavior of Protein on Different Samples

Figure 3B shows the adsorption of protein on each group of samples at 2 h. The results showed that the adsorption amount of BSA was in the order of SZ > Ti = PCZ, and the SZ surface possessed the highest amount ($P < 0.001$). The fluorescence results are consistent with the above quantitative results (Figure 3A); that is, compared with that on the surfaces of Ti and PCZ, the adsorption amount of protein on the SZ surface was the highest.

Biological Assessments in vitro

Behavior of HGKs on Different Samples

Cell adhesion, morphology, viability, proliferation, and adhesion activity were monitored to evaluate the impacts of different sample surfaces on the behavior of HGKs (Figure 4).

Cell Adhesion and Morphology Assessment

Cell adhesion and morphology are important components of cell viability, which reflects the cell behavior on the different sample surfaces. As observed in Figure 4A, for the early cell adhesion experiment carried out within 4 h, the number of initially adherent cells increased on all samples throughout the entire duration. Furthermore, the statistical analysis of cell adhesion showed that the SZ surface had the highest number of adherent cells at 2 h among the three groups ($p < 0.01$), although the effect was not significant at other time points (Figure 4B).

Images of cell morphology and growth were taken for each surface using a fluorescence microscope (Figure 4C). After 1 h of culture, all adherent cells had similar morphologies in all groups, with a round conformation and small spreading area. After 2 h, the cells on the surface of Ti formed more filamentous pseudopodia, while those of SZ protruded only a small amount, and the cells on the PCZ surface did not change obviously. At 4 h, HGKs grew in clusters

Table 2 Chemical Element Composition of Ti, PCZ, and SZ Samples

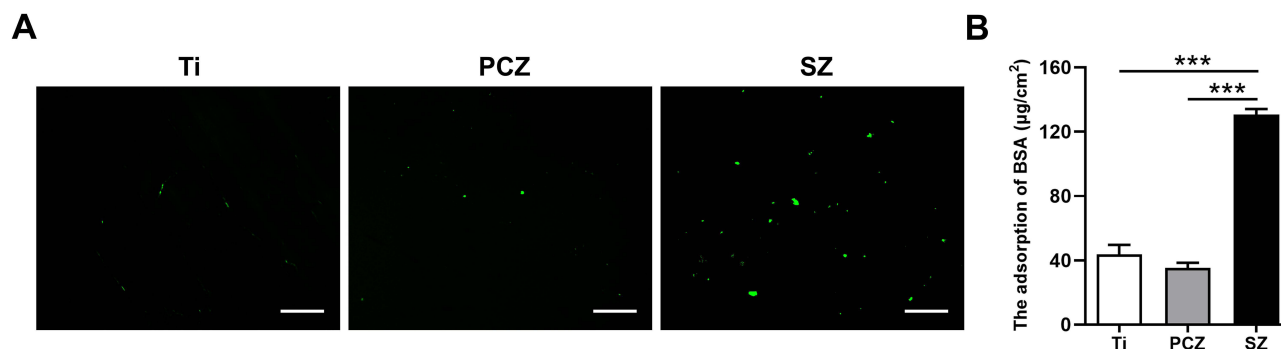| Samples	Elemental Content (at. %)				
	Carbon	**Nitrogen**	**Oxygen**	**Titanium**	**Zirconium**
Ti	1.90	11.98	12.34	71.63	–
PCZ	11.22	9.50	37.46	–	40.75
SZ	14.08	5.36	39.06	–	41.12

Figure 3 Adsorption behavior of BSA on Ti, PCZ, and SZ samples. (**A**) Fluorescence imaging of adsorbed BSA after 2 h culture (scale bar=100μm). (**B**) Adsorption capacity of BSA after 2 h incubation, n=3. ***p<0.001.

and showed comparable morphology among groups. Therefore, these results suggested that the three groups of surfaces have little effect on the morphology of epithelial cells.

Cell Viability and Proliferation Assay

The cell number increased rapidly with time, and there was a similar increase in cell viability at three culture times (Figure 4D), indicating that cell viability was not significantly related to all experimental surfaces. Then, we examined whether the different sample surfaces affected cell proliferation (Figure 4E), and the quantitative analysis results revealed that there were no statistically significant differences among all groups, which was consistent with the cell viability results in general (Figure 4F).

Expression of Adhesion Molecules in HGKs

RT–qPCR was applied to analyze the expression of adhesion molecules at the genetic level. As shown in Figure 4G, the relative expression levels of the adhesion-related genes *Ln α3* and *Ln γ2* were the highest on the SZ surface. In addition, the expression of *Ln β3* and *In α6* on the Ti and SZ surfaces was higher than that on the PCZ surface (p<0.05), whereas there was no significant difference between the Ti and SZ surfaces. All of the above results indicated that the SZ surface induced a superior adhesion activity of HGKs.

The Western blot results also demonstrated that the SZ surface notably upregulated adhesion molecule expression levels of Ln 332, which is consistent with the results of gene-level verification, including the expression of In α6 (p<0.05). However, there was no significant difference in the expression of In β4 between the SZ and PCZ surfaces, but it was higher than that on the Ti surface (Figure 4H and I).

Behavior of HGFs on Different Samples

Cell adhesion, morphology, viability, proliferation, and adhesion activity were analyzed to investigate the impacts of different surfaces on the behavior of HGFs (Figure 5).

Cell Adhesion and Morphology Assessment

The surfaces of the three groups seemed to have no significant effect on the adhesion of HGFs (Figure 5A and B). Moreover, we observed the morphology of HGFs on all surfaces over time. The obtained images showed polygonal cells in all groups after 1 h. After 2 h, cells showed more protruding filamentous pseudopodia and protein filaments. However, cells showed a characteristic morphology of long fusiform shapes in all groups at 4 h. The spreading area of cells was larger, and more protruding pseudopodia were observed on the SZ surface. Therefore, these results suggested that the SZ sample tends to promote the spreading of HGFs (Figure 5C).

Cell Viability and Proliferation Assay

The viability of HGFs on the SZ surface was better than that on the PCZ surface at 3 days (p<0.05), but there was no significant difference among all groups at other time points (Figures 5D). Regarding the cell proliferation behavior, the EdU staining results showed that the rate of positive cells on the SZ surface was higher than that on
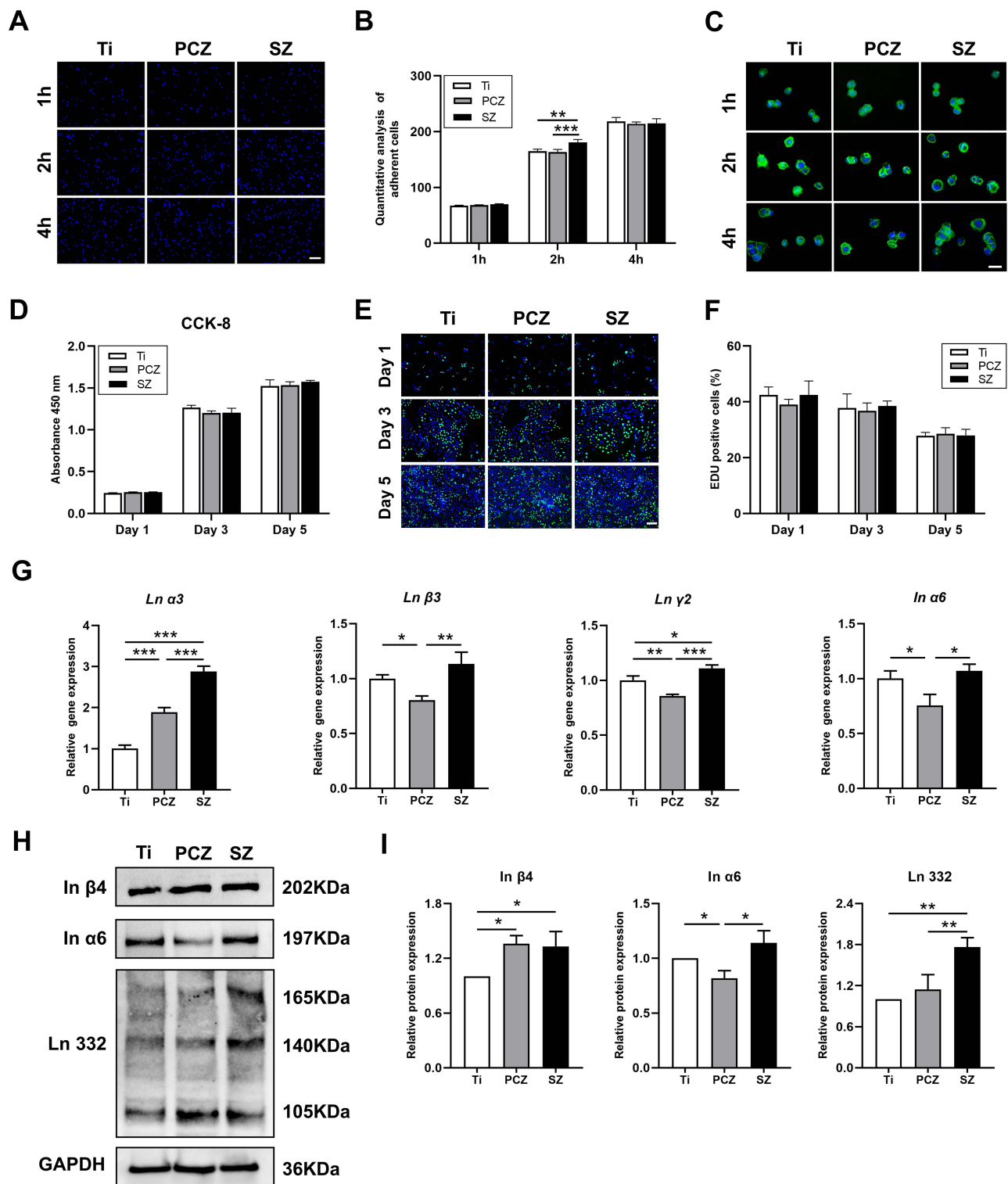
Figure 4 Behavior of human gingival keratinocytes on Ti, PCZ, and SZ samples. (**A** and **B**) Cell adhesion images (scale bar=200μm) and quantitative analysis of adherent cells after 1, 2, and 4 h of seeding, n=3. (**C**) Morphology of adherent cells after 1, 2, and 4 h of seeding, cytoskeleton (green), nuclei (blue), (scale bar=50μm). (**D**) CCK8 assay for cell viability after 1, 3, and 5 days of culture, n=5. (**E** and **F**) Cell proliferation was analyzed by IF staining for EdU after 1, 3, and 5 days of culture (scale bar=200μm) and the graph depicts the percentage of EdU-positive nuclei, proliferative cells (green), nuclei (blue), n=3. (**G**) Adhesion-related genes expression (*Ln α3, Ln β3, Ln γ2 and In α6*) after 3 days of culture, n=3. (**H** and **I**) Representative images and quantitative analysis of adhesion-related proteins expression (Ln 332, In α6 and In β4) after 3 days of culture, n=3. * $p<0.05$, **$p<0.01$, and ***$p<0.001$.

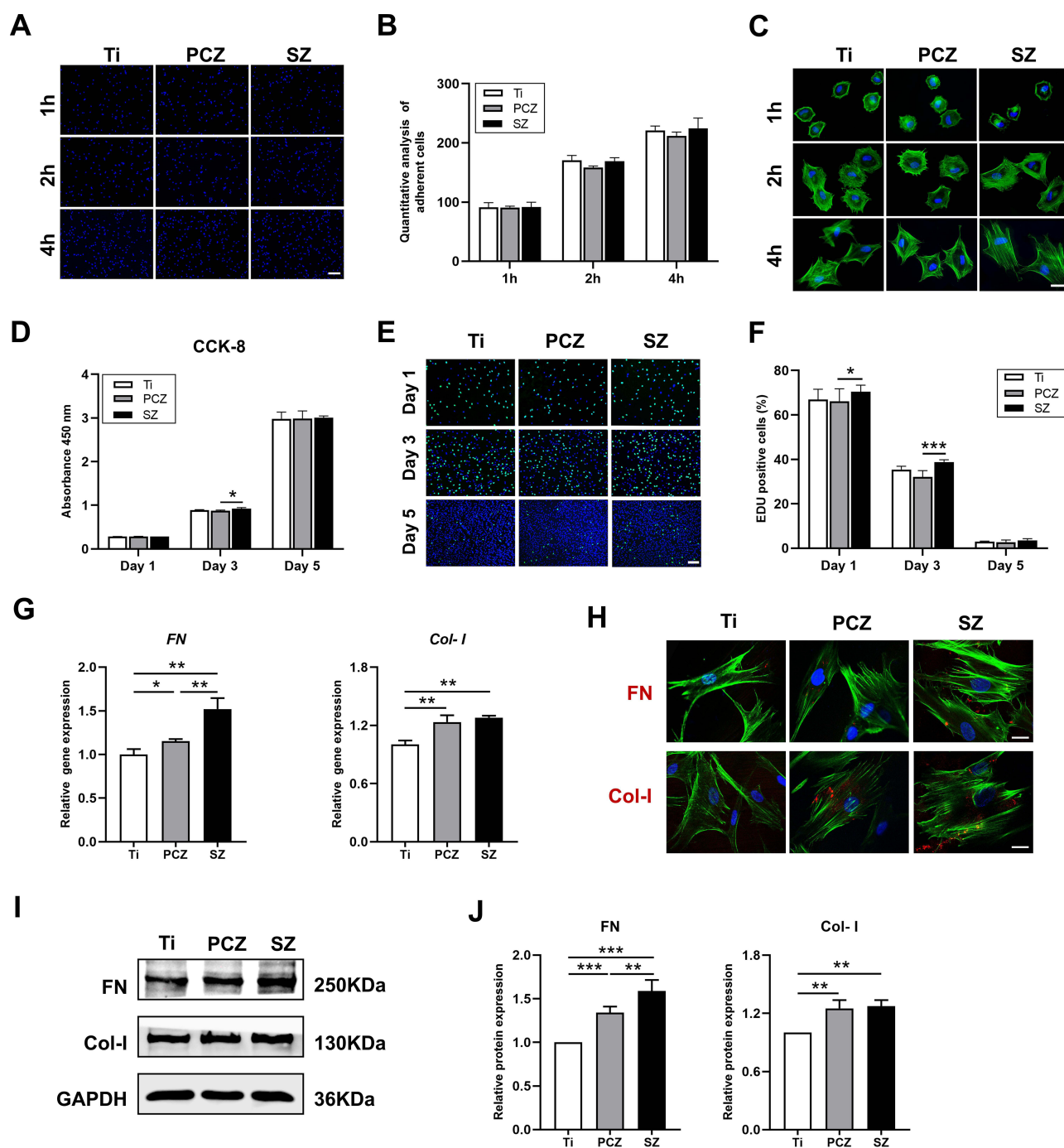**Figure 5** Behavior of human gingival fibroblasts on Ti, PCZ, and SZ samples. (**A** and **B**) Cell adhesion images (scale bar=200μm) and quantitative analysis of adherent cells after 1, 2, and 4 h of seeding, n=3. (**C**) Morphology of adherent cells after 1, 2, and 4 h of seeding, cytoskeleton (green), nuclei (blue), (scale bar=50μm). (**D**) CCK8 assay for cell viability after 1, 3, and 5 days of culture, n=5. (**E** and **F**) Cell proliferation was analyzed by IF staining for EdU after 1, 3, and 5 days of culture (scale bar=200μm) and the graph depicts the percentage of EdU-positive nuclei, proliferative cells (green), nuclei (blue), n=3. (**G**) Adhesion-related gene expression *(Col-I and Fn)* after 3 days of culture, n=3. (**H**) Representative IF staining images of Col-I and Fn; adhesion-related proteins (red), cytoskeleton (green), nuclei (blue), (scale bar=100 μm). (**I** and **J**) Representative images and quantitative analysis of adhesion-related proteins expression (Col-I and Fn) after 3 days of culture, n=3. *$p<0.05$, **$p<0.01$, and ***$p<0.001$.

the PCZ surface at 1 and 3 days ($p<0.05$), whereas cell proliferation basically stopped at 5 days (Figures 5E–F). These results indicated that the SZ surface promotes HGFs viability and proliferation at the initial stage of cell adhesion compared to the PCZ surface.

Expression of Adhesion Molecules in HGFs

As shown in Figure 5G, HGFs on the SZ surface more strongly expressed *FN* than those on the other surfaces. The expression of *Col-I* on the SZ and PCZ surfaces was higher than that on the Ti surface ($p<0.05$), whereas no obvious differences were observed between the SZ and PCZ surfaces.

Compared with those cultured on the Ti and PCZ surfaces, HGFs cultured on the SZ surface expressed more FN ($p<0.05$), but there were no statistically significant differences in Col-I expression between the SZ and PCZ surfaces (Figure 5I and J). IF staining images of FN and Col-I showed that round spots were mainly diffused intracellularly and at the boundary of the cell, and the results are consistent with the Western blot results (Figure 5H).

Biological Assessments in vivo

Hemidesmosome structures and the important adhesion molecule Ln 332 were detected to assess the soft tissue integration of the different abutment surfaces (Figure 2).

Histological Evaluation and Hemidesmosomes Detection

As shown in Figure 2C, H&E stain was used to evaluate the peri-implant soft tissue 4 weeks after the operation. Images showed that the soft tissue around all the abutments healed well. Furthermore, we examined the details of the adhesion structures with hemidesmosomes between the abutments and peri-implant soft tissue by TEM (Figure 2D). It was clearly observed that hemidesmosomes that presented a densely spotted structure formed on the SZ surface. However, there was a small amount of this structure on the Ti surface, while it was almost completely absent on the PCZ surface. This result revealed that the SZ surface may promote hemidesmosome formation at the abutment–gingival interface, which ensures the sealing of soft tissue.

Ln 332 Expression Around the Abutment Surfaces

In vivo immunohistochemical (IHC) staining experiments showed that Ln 332 appeared between the junctional epithelium and the abutment (Figure 2F and G), and a great difference was observed in the expression of Ln 332 among all groups. Apparent positive staining of Ln 332 in the SZ group was observed, whereas low Ln 332 expression was observed for the PCZ and Ti groups. The statistical analysis revealed that the order of positive staining of Ln 332 was SZ >Ti=PCZ ($P < 0.001$). Moreover, Ln 332 expression and distribution were detected by IF staining, and the results are consistent with the IHC results (Figure 2E).

Discussion

Dental abutments are anchored in peri-implant soft tissue, which achieves the formation of a biological seal and then protects the implants from the highly contaminated oral environment.[22] Due to the several limitations of titanium abutments, zirconia is now regarded as one of the best alternatives, especially in applications around the aesthetic zone.[34,35] Nanotopography is currently considered a promising approach for surface design and can regulate bacterial adhesion and cell responses.[27,28] In this study, we presented a novel surface of SZ with nanotopography and explored its soft tissue integration capability compared to Ti and PCZ surfaces to provide a basis for advancing the development of an ideal abutment surface. We found that the SZ surface with nanotopography demonstrated superior soft tissue integration among all samples, which was consistent with our hypothesis.

Following the implantation of dental abutments, the first step that occurs is the adsorption of salivary proteins, which then has a significant effect on subsequent cell behavior,[29,36] and is considered to be a determining factor of cell-biomaterial interactions.[37,38] Previous studies have revealed that the alteration of surface characteristics, such as topography, chemical composition, roughness, and wettability, enables the modulation of protein adsorption and conformation.[36,39–41] In general, proteins tend to be adsorbed on hydrophobic surfaces, and the surface nanotopography can promote the adsorption of proteins, which is consistent with our results.[39,42] In this study, the water contact angle on the SZ surface was the largest and had surface nanotopography, so the adsorption of BSA was highest on the SZ surface. The water contact angle of the PCZ surface was larger than that of the Ti surface, while there was no significant difference between the two groups of surfaces for protein adsorption, which was mainly due to the flat surface after polishing treatment. In addition, we also examined the surface roughness and chemical composition of all samples and

found that the surfaces roughness of the three groups of surfaces were all in the nm ranges, and the difference in Ra value was small. The main chemical composition of PCZ and SZ surfaces were the same and the contents were similar, which indicated that the surface roughness and chemical composition were not the main reasons for the difference in protein adsorption capacity. The SZ surface enhanced protein adsorption, as the medium of cells adhering to the substrate plays a critical role in subsequent cell behavior.

The peri-implant epithelium is the first barrier for protecting the implant from bacterial contamination. When the epithelium attaches to the surface of the abutment, it first forms a basal lamina, and then the epithelial cells attach to the surface through hemidesmosomes. In addition, epithelial cells produce laminin, which ensures the effective attachment of epithelial cells to the abutment surface with the basal lamina.[43] Therefore, we first studied the effects of the three groups of surfaces on epithelial cells.[44] Despite being a cell line, HGKs exhibit typical epithelial cell traits, including the expression of cytokeratin. In the study of HGKs, the SZ surface seemed to promote cell adhesion. And the HGKs on the Ti surface had more filamentous pseudopodia, which may be related to hydrophilicity.[45,46] However, the cell viability or proliferation was not affected regardless of the surface group. Remarkably, we observed obvious differences in the expression of Ln 332 among the three surfaces. Compared with the Ti and PCZ surfaces, the SZ surface not only upregulated the expression of Ln 332, which is the major component of the internal basal lamina and participates in the formation of hemidesmosomes but also had a high expression of In $\alpha6\beta4$, which has a central role in hemidesmosome assembly.[47] The expression of adhesion molecules is an important factor in soft tissue sealing.[48] The results of this study indicated that HGKs cultured on SZ surfaces with nanotopography could achieve ideal epithelial sealing.

Soft tissue integration depends not only on the epithelial attachment but also on the reconstruction of connective tissue attachment to firmly support the epithelial barrier to maintain the long-term success of implants.[49] Thus, we studied the effects of different sample surfaces on HGFs. Researchers have found that titanium with hybrid micro/nanotopographies can reduce inflammatory responses by affecting the state of cell adhesion compared to surfaces with solely microscale topographies. In other words, nanostructures have an edge over regulating cell responses by orchestrating cell adhesion.[50] The SZ surface with nanotopography studied in the paper did not have an obvious regulatory effect on HGFs adhesion, which may be because of the multiple types of regulation induced by different surface properties.[51] Furthermore, cell morphology is also important in determining cell adhesion. Research shows that cells adhered to a nanosurface presented a spreading shape and more projections.[52] The results of this study showed that HGFs exhibited a good spreading morphology on the SZ surface, indicating that the SZ surface with nanotopography promoted cell spreading,[53] but the results seemed to be different for different cells. Additionally, a subtle difference was observed for the SZ surface during the initial incubation time, revealing that the SZ surface may promote viability and proliferation at the initial stage of cell adhesion. It is worth noting that, compared with those on the Ti and PCZ surfaces, the FN expression and secretion on the SZ surface were the highest. These results are in accordance with the IF staining results, which confirm that HGFs cultured on SZ surfaces produce more adhesion molecules, which is beneficial to soft tissue integration.

To further determine the soft tissue sealing ability of the three groups of abutment surfaces, we carried out an animal experiment. Overall, the soft tissue healed well among all abutment surfaces. Furthermore, we analyzed the expression of Ln 332, which is an important adhesion molecule for evaluating epithelial sealing, by IHC and IF staining.[54] In the present study, the signal intensity of Ln 322 on the SZ surface was significantly better than that on the other experimental surfaces. Moreover, the prominent electron-dense plaques of hemidesmosome structures formed on the SZ abutment surface further supported our hypothesis.[43] Therefore, we speculated that these results were obtained under the influence of nanotopography. This provides strong support that the SZ surface has the potential to become a prominent abutment surface.

In this study, the soft tissue integration of the three groups of abutment surfaces was compared in terms of clinical application. SZ was fabricated by additive 3D gel deposition, which forms a dense and homogeneous surface through the dense and uniform deposition of nanoparticles. Different from the unpolished zirconia, the SZ surface has no obvious voids and wear marks in the preparation process, thus achieving a small roughness without polishing treatment.[32,55] The results of this study confirmed that the surface of SZ is effective in soft tissue integration, and the nanotopography seems to be an important influencing factors,[17,56] while the results of titanium and conventional zirconia were comparable,

which is consistent with some previous studies.[15,57] Therefore, the SZ surface is promising and could be applied in more abutments in the future to achieve better biological sealing.

There are some limitations of this study. An ideal abutment surface should simultaneously have soft tissue integration, immunomodulation, and antibacterial properties.[18] In addition, while this abutment surface can absorb more protein, which may be conducive to cell adhesion, it also may induce more bacterial colonization, so it is necessary to carry out more relevant studies to verify the corresponding effects of this surface. Furthermore, the large animal model was not used in this study, and the sample size needs to be increased to be closer to the clinic. And more experiments, such as horseradish peroxidase (HRP) penetration analysis, should be used to further easily visualize the histology and assess the biological sealing capacity of this surface in vivo.[58]

Conclusion

The surface of SZ with nanotopography not only improved protein adsorption but also enhanced the adhesion activity of HGKs and HGFs compared to titanium and conventional zirconia surfaces. In addition, the in vivo results also confirmed that the SZ surface showed better soft tissue integration. From a clinical perspective, the novel SZ may promote biological sealing, which suggests its promising application as a zirconia surface for the dental abutment.

Data Sharing Statement

All relevant data of this study are presented. Additional data will be provided by Chaoyi Huang upon request.

Ethics

The animal experiment was conducted in accordance with the animal care guidelines approved by the the Laboratory Animal Ethics Committee of Guangdong Huawei Testing Co., LTD (approval number: 202203004).

Disclosure

The authors report no conflicts of interest in this work.

References

1. Gibbs S, Roffel S, Meyer M, et al. Biology of soft tissue repair: gingival epithelium in wound healing and attachment to the tooth and abutment surface. *Eur Cell Mater*. 2019;38:63–78. doi:10.22203/eCM.v038a06
2. Ivanovski S, Lee R. Comparison of peri-implant and periodontal marginal soft tissues in health and disease. *Periodontology 2000*. 2018;76 (1):116–130. doi:10.1111/prd.12150
3. Serichetaphongse P, Chengprapakorn W, Thongmeearkom S, et al. Immunohistochemical assessment of the peri-implant soft tissue around different abutment materials: a human study. *Clin Implant Dent Relat Res*. 2020;22(5):638–646. doi:10.1111/cid.12942
4. Ikeda T, Ueno T, Saruta J, et al. Ultraviolet treatment of titanium to enhance adhesion and retention of oral mucosa connective tissue and fibroblasts. *Int J Mol Sci*. 2021;22:22. doi:10.3390/ijms222212396
5. Rezvanian P, Daza R, López PA, et al. Enhanced biological response of AVS-Functionalized Ti-6Al-4V alloy through covalent immobilization of collagen. *Sci Rep*. 2018;8(1):3337. doi:10.1038/s41598-018-21685-3

6. Ajlouni K, Elshahawy W, Ajlouni R, et al. Color masking measurement for ceramic coating of titanium used for dental implants. *J Prosthet Dent*. 2018;119(3):426–431. doi:10.1016/j.prosdent.2017.04.008

7. Shelly S, Liraz Zaltsman S, Ben-Gal O, et al. Potential neurotoxicity of titanium implants: prospective, in-vivo and in-vitro study. *Biomaterials*. 2021;276:121039. doi:10.1016/j.biomaterials.2021.121039

8. Cao Y, Yu C, Wu Y, et al. Long-term survival and peri-implant health of titanium implants with zirconia abutments: a systematic review and meta-analysis. *J Prosthodont*. 2019;28(8):883–892. doi:10.1111/jopr.13097

9. Wang Y, Zhang Y, Sculean A, et al. Macrophage behavior and interplay with gingival fibroblasts cultured on six commercially available titanium, zirconium, and titanium-zirconium dental implants. *Clin Oral Investig*. 2019;23(8):3219–3227. doi:10.1007/s00784-018-2736-z

10. Cosgarea R, Gasparik C, Dudea D, et al. Peri-implant soft tissue colour around titanium and zirconia abutments: a prospective randomized controlled clinical study. *Clin Oral Implants Res*. 2015;26(5):537–544. doi:10.1111/clr.12440

11. Al Rezk F, Trimpou G, Lauer HC, et al. Response of soft tissue to different abutment materials with different surface topographies: a review of the literature. *Gen Dent*. 2018;66(1):18–25.

12. Atsuta I, Ayukawa Y, Furuhashi A, et al. Epithelial sealing effectiveness against titanium or zirconia implants surface. *J Biomed Mater Res A*. 2019;107(7):1379–1385. doi:10.1002/jbm.a.36651

13. Atsuta I, Narimatsu I, Morimoto T, et al. Assessment of the soft-tissue seal at the interface between the base of the fixed denture pontic and the oral mucosa. *Materials*. 2021;14(14):3997. doi:10.3390/ma14143997

14. Wang M, Zhang S, Chen L, et al. Early soft tissue response to zirconium oxide and titanium healing abutments in vivo: a study in dogs. *BMC Oral Health*. 2021;21(1):416. doi:10.1186/s12903-021-01748-0

15. Afrashtehfar KI, Del Fabbro M. Clinical performance of zirconia implants: a meta-review. *J Prosthet Dent*. 2020;123(3):419–426. doi:10.1016/j.prosdent.2019.05.017

16. Li L, Yao L, Wang H, et al. Magnetron sputtering of strontium nanolayer on zirconia implant to enhance osteogenesis. *Mater Sci Eng C Mater Biol Appl*. 2021;127:112191. doi:10.1016/j.msec.2021.112191

17. Guo T, Gulati K, Arora H, et al. Orchestrating soft tissue integration at the transmucosal region of titanium implants. *Acta Biomater*. 2021;124:33–49. doi:10.1016/j.actbio.2021.01.001

18. Chopra D, Gulati K, Ivanovski S. Understanding and optimizing the antibacterial functions of anodized nano-engineered titanium implants. *Acta Biomater*. 2021;127:80–101. doi:10.1016/j.actbio.2021.03.027

19. Chopra D, Gulati K, Ivanovski S. Micro + nano: conserving the gold standard microroughness to nanoengineer zirconium dental implants. *ACS Biomater Sci Eng*. 2021;7(7):3069–3074. doi:10.1021/acsbiomaterials.1c00356

20. Manivasagam VK, Perumal G, Arora HS, et al. Enhanced antibacterial properties on superhydrophobic micro-nano structured titanium surface. *J Biomed Mater Res A*. 2022;110(7):1314–1328. doi:10.1002/jbm.a.37375

21. Kumar S, Nehra M, Kedia D, et al. Nanotechnology-based biomaterials for orthopaedic applications: recent advances and future prospects. *Mater Sci Eng C Mater Biol Appl*. 2020;106:110154.

22. Kim JC, Lee M, Yeo IL. Three interfaces of the dental implant system and their clinical effects on hard and soft tissues. *Mater Horiz*. 2022;9(5):1387–1411. doi:10.1039/D1MH01621K

23. Spitznagel FA, Boldt J, Gierthmuehlen PC. CAD/CAM ceramic restorative materials for natural teeth. *J Dent Res*. 2018;97(10):1082–1091. doi:10.1177/0022034518779759

24. Shen JZ, Zhao J; Hangzhou Erran Technology Co Ltd. Dental all-ceramic restoration and manufacturing method thereof. US patent EP3181090. 2022 April 27.

25. Wu L, Sun Z, Zhao J, et al. Retrospective clinical study of monolithic zirconia crowns fabricated with a straightforward completely digital workflow. *J Prosthet Dent*. 2021;128:913–918. doi:10.1016/j.prosdent.2021.01.018

26. Li Y, Zhao J, Sun Z, et al. Three-dimensional fit of self-glazed zirconia monolithic crowns fabricated by wet deposition. *Dent Mater J*. 2022;41(3):363–367. doi:10.4012/dmj.2021-236

27. Wen C, Muhetaer HJ, Gao Z, et al. Dual response of fibroblasts viability and Porphyromonas gingivalis adhesion on nanostructured zirconia abutment surfaces. *J Biomed Mater Res A*. 2022;110(10):1645–1654. doi:10.1002/jbm.a.37414

28. Wu J, Yu P, Lv H, et al. Nanostructured zirconia surfaces regulate human gingival fibroblasts behavior through differential modulation of macrophage polarization. *Front Bioeng Biotechnol*. 2020;8:611684. doi:10.3389/fbioe.2020.611684

29. Luo J, Walker M, Xiao Y, et al. The influence of nanotopography on cell behaviour through interactions with the extracellular matrix - A review. *Bioact Mater*. 2022;15:145–159. doi:10.1016/j.bioactmat.2021.11.024

30. Sun L, Hong G, Matsui H, et al. The effects of syndecan on osteoblastic cell adhesion onto nano-zirconia surface. *Int J Nanomedicine*. 2020;15:5061–5072. doi:10.2147/IJN.S263053

31. Sun Z, Shen Z, Zhao J, et al. Adaptation and uniformity of monolithic zirconia crowns fabricated by additive 3-dimensional gel deposition. *J Prosthet Dent*. 2022. doi:10.1016/j.prosdent.2021.11.023

32. Rabel K, Nold J, Pehlke D, et al. Zirconia fixed dental prostheses fabricated by 3D gel deposition show higher fracture strength than conventionally milled counterparts. *J Mech Behav Biomed Mater*. 2022;135:105456. doi:10.1016/j.jmbbm.2022.105456

33. Zhang J, Wang H, Wang Y, et al. Substrate-mediated gene transduction of LAMA3 for promoting biological sealing between titanium surface and gingival epithelium. *Colloids Surf B Biointerfaces*. 2018;161:314–323. doi:10.1016/j.colsurfb.2017.10.030

34. Han J, Zhang F, Van Meerbeek B, et al. Laser surface texturing of zirconia-based ceramics for dental applications: a review. *Mater Sci Eng C Mater Biol Appl*. 2021;123:112034. doi:10.1016/j.msec.2021.112034

35. Rajan ST, Terada-Nakaishi M, Chen P, et al. Zirconium-based metallic glass and zirconia coatings to inhibit bone formation on titanium. *Biomed Mater*. 2020;15(6):065019. doi:10.1088/1748-605X/aba23a

36. Barberi J, Spriano S. Titanium and protein adsorption: an overview of mechanisms and effects of surface features. *Materials*. 2021;14(7):1590. doi:10.3390/ma14071590

37. Williams DF. Biocompatibility pathways: biomaterials-induced sterile inflammation, mechanotransduction, and principles of biocompatibility control. *ACS Biomater Sci Eng*. 2017;3(1):2–35. doi:10.1021/acsbiomaterials.6b00607

38. Parisi L, Ghezzi B, Bianchi MG, et al. Titanium dental implants hydrophilicity promotes preferential serum fibronectin over albumin competitive adsorption modulating early cell response. *Mater Sci Eng C Mater Biol Appl*. 2020;117:111307. doi:10.1016/j.msec.2020.111307

39. Lu X, Xiong S, Chen Y, et al. Effects of statherin on the biological properties of titanium metals subjected to different surface modification. *Colloids Surf B Biointerfaces*. 2020;188:110783. doi:10.1016/j.colsurfb.2020.110783

40. Roach P, Farrar D, Perry CC. Interpretation of protein adsorption: surface-induced conformational changes. *J Am Chem Soc*. 2005;127 (22):8168–8173. doi:10.1021/ja042898o

41. Xiao M, Biao M, Chen Y, et al. Regulating the osteogenic function of rhBMP 2 by different titanium surface properties. *J Biomed Mater Res A*. 2016;104(8):1882–1893. doi:10.1002/jbm.a.35719

42. Liddell RS, Ajami E, Li Y, et al. The influence of implant design on the kinetics of osseointegration and bone Anchorage homeostasis. *Acta Biomater*. 2021;121:514–526. doi:10.1016/j.actbio.2020.11.043

43. Fischer NG, Aparicio C. Junctional epithelium and hemidesmosomes: tape and rivets for solving the "percutaneous device dilemma" in dental and other permanent implants. *Bioact Mater*. 2022;18:178–198. doi:10.1016/j.bioactmat.2022.03.019

44. Guo T, Gulati K, Arora H, et al. Race to invade: understanding soft tissue integration at the transmucosal region of titanium dental implants. *Dent Mater*. 2021;37(5):816–831. doi:10.1016/j.dental.2021.02.005

45. Wang C, Wang X, Lu R, et al. Responses of human gingival fibroblasts to superhydrophilic hydrogenated titanium dioxide nanotubes. *Colloids Surf B Biointerfaces*. 2021;198:111489. doi:10.1016/j.colsurfb.2020.111489

46. Zhao X, Cai D, Hu J, et al. A high-hydrophilic Cu(2) O-TiO(2)/Ti(2)O(3)/TiOcoating on Ti-5Cu alloy: perfect antibacterial property and rapid endothelialization potential. *Biomater Adv*. 2022;140:213044. doi:10.1016/j.bioadv.2022.213044

47. Litjens SH, de Pereda JM, Sonnenberg A. Current insights into the formation and breakdown of hemidesmosomes. *Trends Cell Biol*. 2006;16 (7):376–383. doi:10.1016/j.tcb.2006.05.004

48. Lee DJ, Ryu JS, Shimono M, et al. Differential healing patterns of mucosal seal on zirconia and titanium implant. *Front Physiol*. 2019;10:796. doi:10.3389/fphys.2019.00796

49. Nojiri T, Chen CY, Kim DM, et al. Establishment of perpendicular protrusion of type I collagen on TiO(2) nanotube surface as a priming site of peri-implant connective fibers. *J Nanobiotechnology*. 2019;17(1):34. doi:10.1186/s12951-019-0467-1

50. Yang Y, Lin Y, Xu R, et al. Micro/nanostructured topography on titanium orchestrates dendritic cell adhesion and activation via β2 integrin-FAK signals. *Int J Nanomedicine*. 2022;17:5117–5136. doi:10.2147/IJN.S381222

51. Halim FC, Pesce P, De Angelis N, et al. Comparison of the clinical outcomes of titanium and zirconia implant abutments: a systematic review of systematic reviews. *J Clin Med*. 2022;11(17):5052. doi:10.3390/jcm11175052

52. Miao X, Wang D, Xu L, et al. The response of human osteoblasts, epithelial cells, fibroblasts, macrophages and oral bacteria to nanostructured titanium surfaces: a systematic study. *Int J Nanomedicine*. 2017;12:1415–1430. doi:10.2147/IJN.S126760

53. Luo J, Zhao S, Gao X, et al. TiO(2) nanotopography-driven osteoblast adhesion through Coulomb's force evolution. *ACS Appl Mater Interfaces*. 2022;14(30):34400–34414. doi:10.1021/acsami.2c07652

54. Atsuta I, Yamaza T, Yoshinari M, et al. Ultrastructural localization of laminin-5 (gamma2 chain) in the rat peri-implant oral mucosa around a titanium-dental implant by immuno-electron microscopy. *Biomaterials*. 2005;26(32):6280–6287. doi:10.1016/j.biomaterials.2005.03.046

55. Cui X, Shen Z, Wang X. Esthetic appearances of anatomic contour zirconia crowns made by additive wet deposition and subtractive dry milling: a self-controlled clinical trial. *J Prosthet Dent*. 2020;123(3):442–448. doi:10.1016/j.prosdent.2019.02.016

56. Harawaza K, Cousins B, Roach P, et al. Modification of the surface nanotopography of implant devices: a translational perspective. *Mater Today Bio*. 2021;12:100152. doi:10.1016/j.mtbio.2021.100152

57. Roehling S, Schlegel KA, Woelfler H, et al. Zirconia compared to titanium dental implants in preclinical studies-A systematic review and meta-analysis. *Clin Oral Implants Res*. 2019;30(5):365–395. doi:10.1111/clr.13425

58. Zhou X, Atsuta I, Ayukawa Y, et al. Effects of different divalent cation hydrothermal treatments of titanium implant surfaces for epithelial tissue sealing. *Materials*. 2020;13(9):1.